Available online at www.sciencedirect.com
SCIENCE DIRECT®
Solid-State Electronics 48 (2004) 575–580
SOLID-STATE ELECTRONICS
www.elsevier.com/locate/sse

Full-band approaches to the electronic properties of nanometer-scale MOS structures

Fabio Sacconi [a], Michael Povolotskyi [a], Aldo Di Carlo [a,*], Paolo Lugli [a], Martin Städele [b]

[a] *INFM, Department of Electronic Engineering, University of Rome "Tor Vergata", Via del Politecnico, 100133 Rome, Italy*
[b] *Infineon Technologies AG, Corporate Research, Munich, Germany*

Received 12 March 2003; received in revised form 27 June 2003; accepted 18 September 2003

Abstract

Using quantum mechanical methods that include the full-band structure of Si and SiO_2, we study two non-classical phenomena that occur in MOS transistors at the nanometer-scale: tunneling through ultrathin oxides and quantum confinement in Si layers. SiO_2 models based on β-cristobalite, β-quartz and tridymite polymorphs have been implemented for the calculation of tunneling current.

Limitations of the effective-mass approximation are investigated. In particular, we obtain good agreement between calculated and measured tunneling current densities for a n-poly-Si/SiO_2/p-Si MOS capacitor and predict the full-band structure in the channels of bulk and double-gate MOSFETs.
© 2003 Elsevier Ltd. All rights reserved.

Keywords: Tunneling; MOS; Full-band simulations

1. Introduction

Due to the steady progress in Si nanotechnology, prototypes of Si MOSFETs with gate lengths well below 20 nm and only 1–2 nm thin gate oxides have already successfully been fabricated and characterized (see, for example, Ref. [1]). Consequently, quantum mechanical effects such as size quantization and gate oxide tunneling have become increasingly important and can affect the device behavior significantly. In device simulations, these non-classical phenomena are often neglected or treated within simplified schemes, for instance the effective-mass approximation (EMA) [2–4]. Ideally, one should try to combine a complete quantum mechanical description with a full-band approach, avoiding the well-known inherent physical limitations of the EMA [3,4].

In this paper, we present a study of quantum effects in Si/SiO_2 heterostructures based on full-band approaches. Two distinct physical problems are considered: calculation of tunneling through very thin oxide layers in MOS capacitors and of quantized states in Si channels. Tunneling currents have been calculated using a state-of-the-art transfer-matrix-type method [5,6] embedded in an accurate semiempirical tight-binding (TB) framework [7]. This three-dimensional approach has several advantages compared with conventional quasi-one-dimensional effective-mass methods [8]; for example, experimentally observed features such as the violation of parallel momentum conservation during the tunneling process [9] or the enhancement of the effective tunnel mass with decreasing oxide thickness [10] can be accounted for, and reflection from the interfaces as well as microscopic features of the oxide such as defects [11] can be included more realistically.

The second phenomenon studied in this paper is the quantization of Si states in the channel of bulk and Silicon-on-insulator MOSFETs with very thin channels.

* Corresponding author. Tel.: +39-6-72597456; fax: +39-6-2020519.
E-mail address: dicarlo@ing.uniroma2.it (A. Di Carlo).

0038-1101/$ - see front matter © 2003 Elsevier Ltd. All rights reserved.
doi:10.1016/j.sse.2003.09.032

We have used a recently developed linear combination of bulk Bloch states method [12] based on empirical pseudopotential band structures. This approach (in the following called EPM) has been already successfully applied to GaAs/AlAs quantum wells [12]. We compare quantization energies, band dispersions and densities of states obtained with this method with corresponding effective-mass-based results.

2. Full-band approach to oxide tunnelling

To calculate direct tunneling currents through ultra-thin oxide layers in Si/SiO_2 MOS structures, we have followed a methodology which has been described in detail in Refs. [6,8].

Although SiO_2 oxide films on a Si wafer are to be considered amorphous, experimental results [13,14] suggest that some crystalline phases exist at a certain ratio in the dioxide region near the interface. On the ground of these experimental findings and due to the inherent complexity of an atomistic description of amorphous systems, we represented SiO_2 with a suitably chosen periodic structure. In a first step, we constructed microscopic Si[1 0 0]/β-cristobalite–SiO_2/Si[1 0 0] models (see Fig. 1), similar to the ones described in Ref. [15]. The corresponding unit cells have lateral sizes of 0.543 nm × 0.543 nm and SiO_2 thicknesses of $t_{ox} = 0.83$ nm + nc, where n is an integer varying between 1 and 4, and c is the lattice parameter of the bulk oxide, equal to 0.74 nm. All the structures are repeated periodically in a plane parallel to the interfaces. Recent experimental studies [16] and density-functional calculations [17,18] suggested the presence of an interface region about 0.4 nm wide which corresponds, in our microscopical structure, to the non-stoichiometric oxide interface region between Si and β-cristobalite. In the following, we consider as oxide thickness (t_{ox}) the thickness of the stoichiometric oxide layer, as shown in Fig. 1.

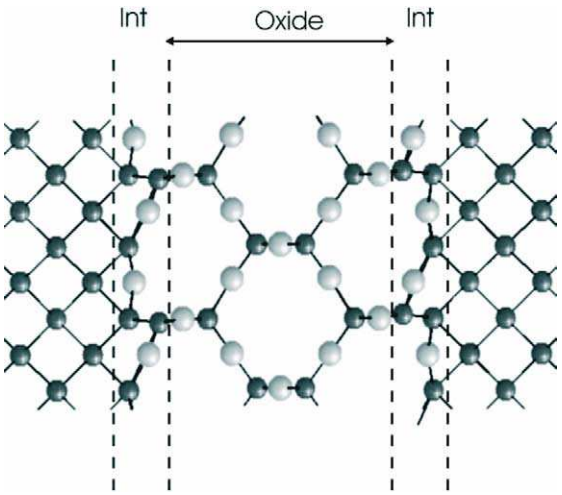

Fig. 1. Model of a typical 0.8 nm thin Si[1 0 0]–SiO_2–Si[1 0 0] model heterojunction based on the β-cristobalite polytype of SiO_2.

Semiempirical sp^3 tight-binding parameters for the cristobalite SiO_2 units were determined to reproduce first-principles full-potential-linearized-augmented-plane-wave (FLAPW) [19] band dispersions as well as the experimental oxide gap of ~9 eV. The effective mass at the minimum of the lowest conduction band of the cristobalite models is found to be $0.34m_0$. For Si, we utilize the highly accurate $sp^3s^*d^5$ parameterization of Ref. [7]. Energy- and parallel-wavevector-dependent transmission coefficients $T(E, k_\parallel)$ were determined from a transfer-matrix-type scheme. To obtain the band profiles of the MOS capacitors, self-consistent solutions of the Schrödinger and Poisson equations have been performed.

The currents were subsequently obtained through the formula

$$J = \frac{-e}{(2\pi)^2\hbar}\int_{BZ_\parallel} \mathrm{d}k_\parallel \int T(E,k_\parallel)[f_R(E,E_{FR}) - f_L(E,E_{FL})]\,\mathrm{d}E, \quad (1)$$

where $T(E, k_\parallel)$ is the transmission coefficient, $BZ_\parallel$ is the two-dimensional Brillouin zone parallel to the interface plane, E_{FL} the Fermi level in the cathode (the poly-Si gate) and E_{FR} the Fermi level in p-Si. A fully numerical $k_\parallel$ integration in the irreducible region of the $BZ_\parallel$ was carried out. We have also calculated currents for the two SiO_2 models whose transmission was already investigated in Ref. [6]: a β-quartz model, with a conduction band mass of $0.62m_0$ and unit cells of 0.543 nm × 0.543 nm and SiO_2 thicknesses between 1.0 and 4.4 nm, and a tridymite model with a conduction band mass of $0.41m_0$ and unit cells of 0.768 nm × 0.768 nm and SiO_2 thicknesses between 0.73 and 4.6 nm.

For the calculation of the tunneling currents we considered a n-poly-Si/SiO_2/p-Si capacitor with a negative voltage applied to the gate terminal, as studied experimentally in Ref. [20]. In accord with the experimental conditions of Ref. [20], an n-doped poly-Si gate with an impurity concentration of 3×10^{20} cm^{-3} and a background dopant concentration of 10^{15} cm^{-3} were assumed. In the following, TB results are compared with calculations performed with a standard transfer matrix approach in EMA [21], both with ("non-parabolic EMA") and without ("parabolic EMA") a Franz-type [22] energy-dependent tunnel mass.

We have found that the tunnel current from the gate is dominated, as expected, by conduction band electrons (CBE), for low oxide voltage, while valence band electrons (VBE) component becomes comparable to CBE

when $|V_{ox}| > \sim 1.2$ V, as soon as empty states in the CB of the anode have the same energy as occupied states in the VB of the cathode.

In Fig. 2, the TB current density in an β-cristobalite SiO_2 based MOS is compared for an oxide thickness of 3.05 nm with EMA calculations, using both the parabolic and the non-parabolic model. For this oxide thickness, the parabolic model underestimates TB results by one order of magnitude, while the non-parabolic model overestimates TB by more than one order of magnitude. For thinner oxides, the EMA results tend to be somewhat closer to TB, as is shown by the inset of Fig. 2. Here, the oxide thickness dependence of the TB and EMA tunneling current densities, calculated for an oxide voltage $V_{ox} = 1$ V is reported for the β-cristobalite model. EMA and TB become of the same order of magnitude for $t_{ox} \cong 1.57$ nm; then, for decreasing thickness, EMA underestimates TB. The non-parabolic correction, on the other hand, yields always an overestimate of the current, of about one order of magnitude, regardless of the oxide thickness. These discrepancies can be attributed to the methodological differences between a microscopic three-dimensional calculation, which includes an atomistic description of the Si/SiO_2 interface, and the standard effective-mass treatment of the tunneling process [10].

In Fig. 2, the calculations are also compared with experimental data of Ref. [20] for a 2.8-nm thick oxide, and, in the inset, for several oxide thicknesses and for $V_{ox} = 1$ V. It must be noted that, in the TB calculation, t_{ox} varies as an integer multiple of the unit cell length, while experimental data refer to different values for oxide thicknesses. TB calculations show a quite good agreement with experiment, even if in some cases the TB current is somewhat larger than the experimental results, which can be due to the uncertainty in the measured oxide thickness. If the extrapolated current values are assumed to vary according to an exponential law $J(t_{ox}) \propto e^{-t_{ox}}$, we obtain that TB calculations for β-cristobalite deviate from experimental data by a factor that lies between 2 and 7.5.

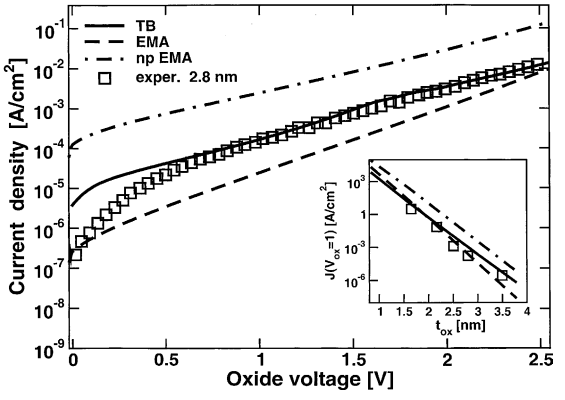

Fig. 2. TB tunneling current density (solid line), compared to EMA (dash dotted line) and non-parabolic EMA (dash line), for 3.05 nm thick β-cristobalite oxide; experimental measurement [20] for $t_{ox} = 2.8$ nm is also shown. The inset shows the calculated and experimental oxide thickness dependences of the current density for $V_{ox} = 1$.

Calculations performed with the other two SiO_2 polytypes show a good agreement of tridymite model with experiments in Ref. [20], while the β-quartz values are at least two orders of magnitude lower. This is plausible because the β-quartz model has the largest ($0.62m_0$) conduction band mass (and, related to that, also the largest tunnel mass). On the other hand, calculations in Ref. [10] yield absolute values for experimental tunnel masses that are closest to the absolute tridymite masses. We note that the calculated currents of all the three SiO_2 polytypes depend exponentially on the oxide thickness, in agreement with the experimental results reported in Refs. [20,23]. Details of these results will be published elsewhere.

3. Full-band approach to quantized states in Si layers

A linear combination of bulk Bloch states method is used for the calculation of the single-particle electronic states of the Si/SiO_2 nanostructures. The one-particle Hamiltonian is expressed in terms of the empirical pseudopotentials of the constituent atoms. We use the approach proposed in Refs. [8,12] with the perodic pseudopotential $V_P^\alpha(\mathbf{r})$, defined as

$$V_P^\alpha(\mathbf{r}) = \sum_{\mathbf{R}} v^\alpha(\mathbf{r} - \mathbf{R}), \tag{2}$$

where $v^\alpha(\mathbf{r})$ is pseudopotential due to a single atom, α is the atom number in the unit cell, $\mathbf{R}$ is a Bravais vector and the summation is performed over the infinite Bravais lattice. We assume that the role of SiO_2 is reduced to the strong confinement of electrons in the Si layer, so the Hamiltonian can be expressed as follows:

$$H = -\frac{\hbar^2}{2m_0}\nabla^2 + \sum_\alpha V_P(\mathbf{r} - \mathbf{d}_\alpha)V_{conf}(\mathbf{r}) + e\varphi(\mathbf{r}), \tag{3}$$

where m_0 is free electron mass, $\mathbf{d}_\alpha$ is the offset of αth atom in the unit cell, $V_{conf}(\mathbf{r})$ is confining potential of SiO_2 and $e\varphi(\mathbf{r})$ is the additional electrostatic energy due to the redistributed free carriers. We approximate confining potential $V_{conf}(\mathbf{r})$ as a rectangular barrier with 3.15 eV height. Pseudopotential values of Si atoms were taken from Ref. [24]. The Silicon conventional unit cell used in the calculations consists of four atoms, in order to have a Bravais vector parallel to the [0 0 1] growth direction [12]. This enables us to define a "perpendicular" one-dimensional space, where the lattice symmetry

is broken, and a "parallel" two-dimensional space where periodicity is preserved. Eigen-function $\psi^{n\mathbf{k}_\parallel}(\mathbf{r})$ of the Hamiltonian (3) were expressed as a linear combination of the bulk Bloch functions $\chi^{\mathbf{k}_\parallel}_{n\mathbf{k}_\perp}(\mathbf{r})$:

$$\psi^{n\mathbf{k}_\parallel}(\mathbf{r}) = \sum_{n\mathbf{k}_\perp} C^{\mathbf{k}_\parallel}_{n\mathbf{k}_\perp} \chi^{\mathbf{k}_\parallel}_{n\mathbf{k}_\perp}(\mathbf{r}) = \sum_{n\mathbf{k}_\perp} C^{\mathbf{k}_\parallel}_{n\mathbf{k}_\perp} \sum_{\mathbf{G}} B_{n\mathbf{k}} e^{i(\mathbf{G}+\mathbf{k})\mathbf{r}}, \quad (4)$$

where n is a bulk band number, $\mathbf{k}_\parallel$ is a wave vector from the 2D Brillouin zone corresponding to the parallel space, $\mathbf{k}_\perp$ is a wave vector parallel to the growth direction, $\mathbf{k} = \mathbf{k}_\perp + \mathbf{k}_\parallel$, $\mathbf{G}$ is a reciprocal lattice vector.

In order to reduce Schrödinger equation $H\psi = E\psi$ to the linear algebra problem we have to calculate matrix elements of the Hamiltonian (3). For them we have:

$$\langle \psi^{n'\mathbf{k}'} | H | \psi^{n\mathbf{k}} \rangle = \delta_{n'\mathbf{k}',n\mathbf{k}} \varepsilon_{n\mathbf{k}} + \langle \psi^{n'\mathbf{k}'} | V_{\text{conf}} | \psi^{n\mathbf{k}} \rangle + \langle \psi^{n'\mathbf{k}'} | e\varphi | \psi^{n\mathbf{k}} \rangle. \quad (5)$$

Calculation of the matrix elements in Eq. (5) is done in the assumptions that electrical potential φ is a smooth function, i.e., its Fourier components belong to the first bulk Brillouin zone, and V_{conf} is a step-like function, constant inside the unit cell. Then, with the use of Fourier transformations $V_{\text{conf}}(\mathbf{k})$ and $\varphi(\mathbf{k})$, the matrix elements are expressed as:

$$\begin{aligned} \langle \psi^{n'\mathbf{k}'} | V_{\text{conf}} | \psi^{n\mathbf{k}} \rangle &= V_{\text{conf}}(\mathbf{k}_\perp - \mathbf{k}'_\perp) \sum_{\mathbf{G},\mathbf{G}'} B^*_{n'\mathbf{k}'}(\mathbf{G}') B_{n\mathbf{k}}(\mathbf{G}) \\ &\quad \times \operatorname{sinc}(\mathbf{k} - \mathbf{k}' + \mathbf{G} - \mathbf{G}'), \\ \langle \psi^{n'\mathbf{k}'} | e\varphi | \psi^{n\mathbf{k}} \rangle &= \varphi(\mathbf{k}_\perp - \mathbf{k}'_\perp) \sum_{\mathbf{G},\mathbf{G}'} B^*_{n'\mathbf{k}'}(\mathbf{G}') B_{n\mathbf{k}}(\mathbf{G}) \\ &\quad \times \operatorname{Rect}_{\mathbf{G}_1,\mathbf{G}_2,\mathbf{G}_3}(\mathbf{k} - \mathbf{k}' + \mathbf{G} - \mathbf{G}'). \end{aligned} \quad (6)$$

For the details, see Ref. [12]. We find that an efficient implementation of this approach, even if coupled self-consistently with the Poisson equation, is possible with a rather small number of Bloch functions included in the basis (200 bulk states for every $k_\parallel$).

Fig. 3 compares the $E(k_\parallel)$ band dispersion of the bound states in the channel of a double-gate MOSFET, obtained with the present full-band method and with the parabolic and non-parabolic EMA for two different directions in reciprocal space ([1 0 0] and [1 1 0]); channel thickness is 2.2 nm. Longitudinal and transversal effective masses were evaluated numerically from the bulk band dispersion, calculated with pseudopotential method. They are found to be equal to $0.92m_0$ and $0.20m_0$ respectively. For the first two levels in the vicinity of the Brillouin zone center, the quantization energies from the two approaches are in quite good agreement, the difference being less than 5 meV. The corresponding differences (at low energies) for a 10 nm wide channel are found to be about one order of magnitude smaller. Note that the levels at $k_\parallel = 0$ appear to be degenerate on the scale of Fig. 3, while there is actually a tiny O (meV) splitting [25]. However, for larger $k_\parallel$ and larger energies (>0.5 eV), the EMA results deviate significantly from the full-band results, leading to a strong overestimate of band dispersions and group velocities; this holds also for the 10.5 nm wide channel. The discrepancies are most salient along the [1 1 0] direction. In particular, the degeneracy of the bands at zero momentum is lifted due to valley interaction effects that the EMA cannot account for.

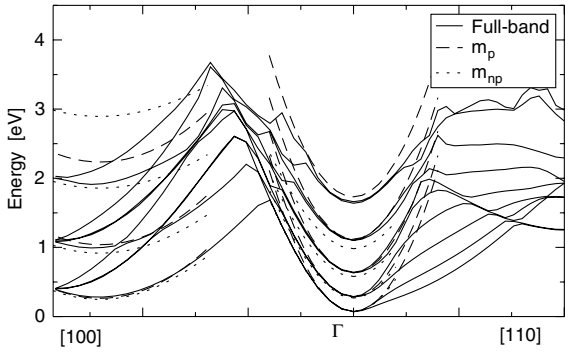

Fig. 3. Band dispersions of bound electronic states in the channel of a double-gate MOSFET for two directions in k-space ([1 0 0] and [1 1 0]). The channel width is equal to 2.2 nm. The comparison of EPM (solid line), EMA (m_p, dashed line) and EMA with non-parabolic corrections (m_{np}, dotted line) is shown.

In order to calculate density of states we introduce a coarse rectangular grid over the irreducible wedge of two-dimensional Brillouin zone which contains about 10^3 grid nodes. For every $k_\parallel$ this grid we calculate about 10^2 eigen-energies and then interpolate results for a denser grid (about 2×10^6 nodes). Then we count number of states in the range between E_0 and $E_0 + \Delta E$ ($\Delta E \sim 1$ meV). These numbers were normalized per unit area and unit of energy, taking into account spin degeneracy. Results were tested for convergence by increasing the number of nodes of both grids.

Fig. 4 compares the density of electron states (DOS) in the channel of a double-gate MOSFET, calculated with the approaches discussed above, for three different channel widths. Neglecting the small details, the DOS turns out to be almost proportional to the channel width in the investigated range (from 2 nm up to 10 nm). The results show that the DOS is underestimated in EMA approach. The DOS of the non-parabolic band model is also shown, which is closer to the full-band calculation than parabolic model. The large discrepancy that remains between pseudopotential and non-parabolic band model is due to the fact that inclusion of non-parabolicity can reproduce the band dispersion only in a particular direction. In our calculation we adjust non-parabolicity parameter in order to have the same band

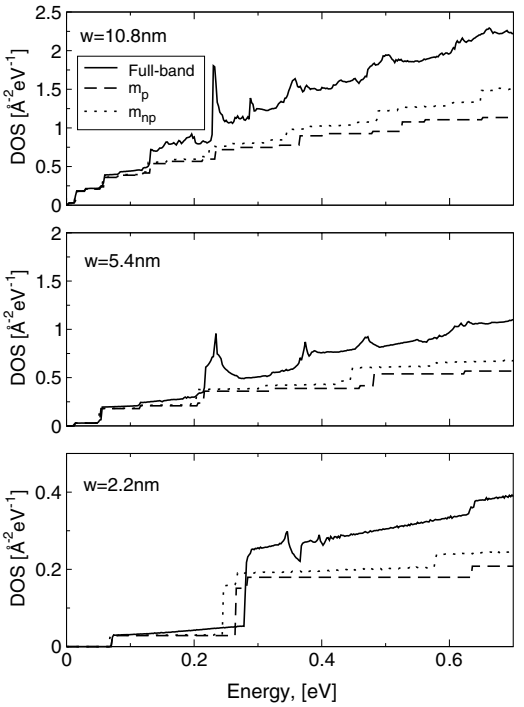

Fig. 4. Sheet density of conduction band states for the channel of a double-gate MOSFET, calculated with EPM, EMA (m_p), and EMA (m_{np}) with non-parabolic corrections. Results for channel widths of 2.2, 5.4 and 10.8 nm are shown.

dispersion in the bulk silicon near conduction band minimum, as calculated by pseudopotential model. Such approach assures that quantization energies of the first levels are correct. However, dispersion for the rest of **k**-space still differs from the full-band results. For example it is not possible to reproduce neither removal of band degeneracy in the [1 1 0] direction (see Fig. 3) nor band coupling effects. Since non-parabolic corrections, being asymptotically proportional to k^4 are valid only around the band minimum, quantization energies starting from the third level are even less accurate that those obtained by a parabolic model. Interestingly, in the 2.2 nm thin double-gate MOSFET channel the difference between the EMA and the full-band DOS is less than 10% for $E < 0.25$ eV. For a larger thickness (10.8 nm), however, the differences are larger (less than 10% difference only for $E < 0.15$ eV).

Qualitatively very similar results are obtained for the inversion layer of the bulk MOSFET, for which we compare the density of electron states (DOS) in Fig. 5, calculated with the various approaches discussed above. In this calculation, the Schrödinger equation was self-consistently coupled with Poisson equation [26,27]. Internal field strength in the channel was found to be equal to 200 kV/cm. As can be expected, the DOS is

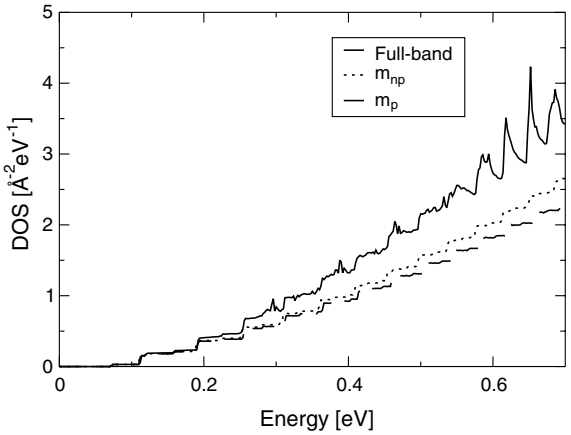

Fig. 5. Sheet density of conduction band states for the inverted channel of a MOSFET, calculated with the empirical pseudopotential method (Full-band), EMA (m_p), and EMA (m_{np}) with non-parabolic corrections.

underestimated in the parabolic EMA. Non-parabolic corrections can only somewhat improve the parabolic results.

Well distinguishable peaks in the DOS (see Figs. 4 and 5) can be ascribed to the complex structure of the 2D bands. Namely, non-monotonic dispersion (see Fig. 3) leads to the existence of particular energy values where the density of states has a local maximum or minimum. Similar peaks were reported for the DOS of a bulk Si in Ref. [28].

Since effective-mass approach underestimates DOS, we can expect, from full-band calculations, higher scattering rates and lower channel mobilities.

4. Conclusions

We have calculated the effects of incorporating full-band treatment into two quantum mechanical simulation approaches for nanometer-scale MOS systems.

It was shown that tunneling currents in MOS structures can be obtained with good accuracy by microscopic calculations based on empirical tight-binding models without any fitting parameters.

The results suggest a strong dependence of tunneling currents on the local oxide structure of the specific SiO_2 polymorph (β-cristobalite, β-quartz or tridymite). Also, effective-mass currents are found to deviate by about one order of magnitude from the tight-binding results.

In addition, a full-band pseudopotential approach has been applied to calculate the band dispersion and DOS for quantized electrons in MOSFET channels. We find that full-band corrections become significant at energies > 0.5 eV and for characteristic inversion channel

widths of a few nm. We expect the non-parabolicity corrections to be even more significant for hole channels.

Acknowledgements

This work has been supported by the Office of Naval Research (ONR) and Progetto 5% Microelettronica.

References

[1] See the Technical Digest of the International Electron Device Meeting (IEDM), San Francisco, 2002.
[2] Duke CB. In: Seitz F, Turnbull D, Ehrenreich H, editors. Tunneling in solids, solid state physics, vol. 10. New York: Academic Press; 1969.
[3] Ivchenko EI, Pikus G. In: Superlattices and other heterostructures. Springer Series in Solid-State Sciences, vol. 110. Berlin: Springer; 1995. p. 73.
[4] Burt MG. J Phys Cond Mat 1999;11:R53.
[5] Strahberger C, Vogl P. Phys Rev B 2000;62:7289.
[6] Städele M, Tuttle BR, Hess K. J Appl Phys 2001;89:348, and references therein.
[7] Jancu JM et al. Phys Rev B 1998;57:6493.
[8] Di Carlo A. Semicond Sci Technol 2003;18:R1.
[9] Weinberg Z, Hartstein A. J Appl Phys 1983;54:2517.
[10] Städele M, Sacconi F, Di Carlo A, Lugli P. J Appl Phys 2003;93:2681.
[11] Städele M, Fischer B, Tuttle B, Hess K. Solid State Electron 2002;46:1027.
[12] Chirico F, Di Carlo A, Lugli P. Phys Rev B 2001;64:045314.
[13] Ikarashi N, Watanabe K, Miyamoto Y. Phys Rev B 2000;62:15989.
[14] Tu Y, Tersoff J. Phys Rev Lett 2000;84:4393.
[15] Ohdomari I et al. J Appl Phys 1987;62:3751.
[16] Muller DA, Sorsch T, Mocio S, Baumann FH, Evans-Lutterodt K, Timp G. Nature 1999;399:758.
[17] Demkov A, Sankey OF. Phys Rev Lett 1999;83:2038.
[18] Demkov A, Zhang X, Drabold DA. Phys Rev B 2001;64:125306.
[19] Blaha P, Schwarz K, Luitz J. WIEN97, a full potential linearized augmented plane wave package for calculating crystal properties. Wien; 1999.
[20] Khairurrjial, Mizubayashi W, Miyazaki S, Hirose M. J Appl Phys 2000;87:3000.
[21] Ando Y, Itoh T. J Appl Phys 1987;61:1497.
[22] Franz W. In: Flügge S, editor. Handbuch der Physik, vol. 17. Berlin: Springer; 1956. p. 206.
[23] Brar B, Wilk GD, Seabaugh AC. Appl Phys Lett 1996;69:2728.
[24] Friedel P, Hybersten MS, Schlüter M. Phys Rev B 1989;39:7974.
[25] Ando T, Fowler AR. Rev Mod Phys 1982;54:437.
[26] Jallepalli S et al. IEEE Trans Electron Dev 1997;44:297.
[27] Takeda H, Mori N, Hamaguchi C. J Comput Electr 2002;1:467.
[28] Fischetti MV, Laux SE. Phys Rev B 1988;38:9721.